Applied Thermal Engineering 288 (2026) 129539

Contents lists available at ScienceDirect

Applied Thermal Engineering

journal homepage: www.elsevier.com/locate/apthermeng

Research Paper

Simulation study of a horizontally installed compact helical earth-air heat exchanger for energy efficiency in buildings

Andre L. Razera [a], Cesare Biserni [b,*], Michel K. Rodrigues [a], Luiz A.O. Rocha [c], Elizaldo D. dos Santos [c], Liércio A. Isoldi [c]

[a] School of Engineering, Universidade Federal do Rio Grande, Rio Grande, RS, Brazil
[b] Alma Mater Studiorum University of Bologna, Bologna, Italy
[c] Graduate Program in Computational Modeling, Universidade Federal do Rio Grande, Rio Grande, RS, Brazil

ARTICLE INFO

Keywords:
Solar energy
Thermal potential
Pressure drop
Multiobjective evaluation (TOPSIS)
Computational fluid dynamic (CFD)

ABSTRACT

This study presents a numerical investigation of a compact Horizontal Helical Earth–Air Heat Exchanger (EAHE-HH), developed for the climatic and soil conditions of Viamão, Brazil. The analysis focuses on the influence of the helical pitch (P_h) on the system's thermal and fluid-dynamic behavior. Simulations were performed in ANSYS Fluent using the Finite Volume Method, and performance was assessed through the thermal potential (*TP*) and pressure drop (*PD*), combined in a multiobjective evaluation using the Technique for Order Preference by Similarity to Ideal Solution method (TOPSIS). Results show that the EAHE-HH is effective for air cooling during warm periods, while its heating capacity remains negligible under local winter conditions. Among the tested configurations, $P_h = 100$ mm provided the highest thermal performance, improving TP by approximately 10 % compared to $P_h = 400$ mm. Conversely, the largest pitch ($P_h = 400$ mm) reduced pressure drop by up to 66 % relative to $P_h = 100$ mm. The EAHE-HH displayed cooling performance comparable to other EAHE systems reported for the same region, supporting its applicability in areas with limited surface availability and reduced excavation requirements. The TOPSIS method has proven effective in evaluating the performance indicators *TP* and *PD*, identifying the best performance at opposite extremes of the geometric range under study.

1. Introduction

There has been a growing emphasis on sustainable air conditioning systems, driven by increasing environmental and energy concerns. This societal shift seeks to reduce electricity consumption, which has risen considerably due to the increasing thermal comfort requirements in residential and commercial buildings [1,2]. In addition, the elevated energy usage of conventional air conditioning systems has significant adverse environmental impacts, particularly with regard to the depletion of the ozone layer and the intensification of global warming [3,4]. Within this context, the Earth-Air Heat Exchanger (EAHE) has emerged as a promising solution to complement traditional air conditioning systems, offering the ability to passively cool and/or heat indoor spaces with minimal environmental impact [5,6].

Solar radiation is a widely available and abundant source of thermal energy. A fraction of this incident energy is absorbed by the ground surface, accumulating in the shallow layers of the soil and gradually establishing a thermal gradient over time [6]. EAHE systems harness this thermal reservoir through ducts installed in the soil, where the forced airflow (generated by blowers or fans) exchanges heat with the surrounding medium [7]. Consequently, the system enables air cooling during periods of high ambient temperatures – typically in summer – and air heating during periods of low temperatures, commonly observed in winter [8,9].

A wide range of design configurations can be adopted for EAHE systems, including vertical or horizontal orientations, as well as series or parallel layouts [10]. Each configuration presents specific characteristics that allow adaptation to the geometric constraints of buildings and plots, while also considering the geotechnical and climatic conditions of each location [11,12]. Vertical EAHE systems require less ground surface area, making them particularly advantageous in space-limited plots or densely built urban areas. However, to achieve enhanced thermal performance, they may require greater installation depths [12]. Several geometric configurations have been investigated for vertical systems, including helical and U-shaped designs [11,13–19]. On the other hand, horizontal EAHE systems can often operate effectively in shallower excavations and support a wide range of configurations, such as straight

* Corresponding author at: Department of Industrial Engineering, Alma Mater Studiorum-University of Bologna, Viale Risorgimento 2, 40136 Bologna, Italy.
E-mail address: cesare.biserni@unibo.it (C. Biserni).

https://doi.org/10.1016/j.applthermaleng.2025.129539
Received 8 October 2025; Received in revised form 2 December 2025; Accepted 17 December 2025
Available online 22 December 2025

Nomenclature

C_i	TOPSIS multiobjective indicator
C_p	Specific heat at constant pressure (J/(kg·K))
D	Diameter of the helical coil (m or mm)
d	Internal diameter of the duct (m or mm)
H_s	Soil depth (m or mm)
k	Thermal conductivity (W/(m·K))
L	Helical length (m or mm)
L_c	Helical center depth (m or mm)
L_d	Duct length (m or mm)
L_s	Soil length (m or mm)
L_{sup}	Top helical depth (m or mm)
L_T	Total installation depth (m or mm)
PD	Pressure drop (N m^{-2})
P_h	Helical pitch (m or mm)
P_{in}	Inlet pressure (N m^{-2})
P_o	Outlet pressure (N m^{-2})
Re	Reynolds number
T	Temperature (K or °C)
t	Time (s)
TP	Thermal potential (K or °C)
v	Velocity (m/s)
w_1	Thermal weight
w_2	Fluid dynamic weight
W_s	Soil width (m or mm)

Greek symbols

μ	Dynamic viscosity (kg/(m·s))
ν	Kinematic viscosity (m^2 s^{-1})
ρ	Density (kg m^{-3})
α	Thermal diffusivity (m^2 s^{-1})

Subscripts/Superscripts

CP	Central plane
d	Duct
in	Inlet
o	Outlet
S	Soil
(−)	Spatial-averaged variables
(−5d)	Five-day averaged
(−M)	Month averaged
Est	Estimation
Ref	Reference

Abbreviations

EAHE	Earth-Air Heat Exchanger
EAHE-HH	Horizontal Helical Earth-Air Heat Exchanger
EAHE-VH	Vertical Helical Earth-Air Heat Exchanger
EAHE-HR	Rectilinear Horizontal Earth-Air Heat Exchanger
EAHE-V3U	Vertical 3U-shaped Earth-Air Heat Exchanger
TOPSIS	Technique for Order Preference by Similarity to Ideal Solution

ducts, multiple parallel ducts, T-Shaped or Y-Shaped layouts, U-Shaped arrangements, and serpentine patterns, among others [14,17,20–25]. Although horizontal systems typically require larger surface areas for installation, certain configurations – such as the helical geometry – show promising potential by enabling more compact layouts. In this context, such solutions warrant further investigation for applications in spatially constrained environments.

As discussed by Rodrigues et al. [20], the performance evaluation of different EAHE configurations can be based on two main parameters: the thermal potential (*TP*), representing the temperature variation of the air between the duct's inlet and outlet; and the pressure drop (*PD*), associated with the pressure difference along the system, both commonly used indicators in EAHE assessments. Besides that, a multiobjective analysis can be conducted using the Technique for Order Preference by Similarity to Ideal Solution method (TOPSIS) [26], which integrates the *TP* and *PD* metrics under different weighting schemes assigned to each performance criterion. The use of this approach has yielded consistent results in studies addressing both thermal and fluid dynamic performance [22,27–30].

Considering these aspects, this study presents a numerical analysis of a Horizontal Helical EAHE, considering the subtropical climate and soil thermal properties of Viamão, Rio Grande do Sul, Brazil. Unlike other studies available in literature, this work adopts a compact horizontal helical configuration, characterized by the requirement of a smaller surface area and shallower installation depth, a key distinguishing aspect of the proposed system. To this end, the geometry of the system is assessed by varying the pitch between the helicoids (P_h), while keeping the flow and installation conditions constant across all cases, except for the total duct length, which changes according to the selected P_h. Lastly, the EAHE-HH results are benchmarked against previous studies on alternative configurations, including the Vertical Helical (EAHE-VH) and Rectilinear Horizontal (EAHE-HR) systems analyzed by Vaz et al. [16], as well as the Vertical EAHE with three U-shaped ducts (EAHE-V3U), investigated by Vaz et al. [13].

In addition to these aspects, it is important to note that the configuration investigated in this work introduces a geometrical arrangement that remains scarcely explored in EAHE studies. The system adopts a horizontal helical layout in which variations of the helical pitch (P_h) act in the lateral direction, in contrast to the vertically oriented helical configurations examined in Vaz et al. [16]. Furthermore, due to its shorter total installation length, the proposed arrangement is considerably more compact than conventional extended horizontal ducts, such as those analyzed by Vaz et al. [16], Rodrigues et al. [20], and Andrade et al. [22]. These features enable installation in areas with limited surface availability and restricted excavation depth, being conditions typically found in densely built urban environments. Consequently, this compact geometry provides a relevant design alternative and offers new insight into how reduced lateral extension and spacing between turns influence the thermal and fluid-dynamic behavior of the EAHE-HH.

2. Mathematical modeling

The mathematical model employed to characterize the thermal and fluid dynamic behavior is based on the fundamental conservation laws of mass, momentum, and energy [31]. The airflow within the duct is considered unsteady, incompressible, and turbulent, with heat transfer governed by forced convection, as in Rodrigues et al. [20]. Under these assumptions, the governing equations are formulated according to the approach presented by Launder and Spalding [32] and Wilcox [33]:

$$\frac{\partial(\overline{v}_i)}{\partial x_i} = 0 \qquad i = 1,2,3 \text{ in } t \times \Omega \tag{1}$$

$$\frac{\partial \overline{v_i}}{\partial t} + \frac{\partial\left(\overline{v_i}\overline{v_j}\right)}{\partial x_j} = -\frac{1}{\overline{\rho}}\frac{\partial \overline{p}}{\partial x_j}\delta_{ij} + \frac{\partial}{\partial x_j}\left[\upsilon\left(\frac{\partial \overline{v_i}}{\partial x_j} + \frac{\partial \overline{v_j}}{\partial x_i}\right) - \tau_{ij}\right] \qquad i,j = 1,2,3 \text{ in } t \times \Omega \tag{2}$$

$$\frac{\partial \overline{T}}{\partial t} + \frac{\partial}{\partial x_j}\left(\overline{v_j}\overline{T}\right) = \frac{\partial}{\partial x_j}\left(\alpha_a \frac{\partial \overline{T}}{\partial x_j} - q_j\right) \qquad i,j = 1,2,3 \text{ in } t \times \Omega \tag{3}$$

the overbar (—) indicates the temporal average. The symbol v refers to the flow velocity, p denotes the static pressure of the fluid, $\delta_{i,j}$ is the

Kronecker delta and. The parameters υ and α_a represent, respectively, the absolute viscosity and thermal diffusivity of the air, both considered constant throughout the analysis. The components τ_{ij} and q_j are modeled by [32,33]:

$$\tau_{i,j} = \overline{v_i' v_j'} \qquad i,j = 1,2,3 \text{ in } t \times \Omega \tag{4}$$

$$q_j = \overline{v_i' T'} \qquad i,j = 1,2,3 \text{ in } t \times \Omega \tag{5}$$

To resolve the closure problem inherent in turbulent flow modeling, the Reynolds-Averaged Navier-Stokes (RANS) k–ε model was adopted [20]. This turbulence model requires the solution of two transport equations: one for the turbulent kinetic energy (k) and another for its rate of dissipation (ε), as proposed by Launder and Spalding [32] and Wilcox [33].

$$\frac{\partial k}{\partial t} + \overline{v}_j \frac{\partial k}{\partial x_j} = \tau_{ij} \frac{\partial \overline{v}_i}{\partial x_j} + \frac{\partial}{\partial x_j}\left[\left(\upsilon + \frac{\upsilon_t}{\sigma_k}\right)\frac{\partial k}{\partial x_j}\right] - \varepsilon \qquad i,j,k = 1,2,3 \text{ in } t \times \Omega \tag{6}$$

$$\frac{\partial \varepsilon}{\partial t} + \overline{v}_j \frac{\partial \varepsilon}{\partial x_j} = \frac{\partial}{\partial x_j}\left[\left(\upsilon + \frac{\upsilon_t}{\sigma_\varepsilon}\right)\frac{\partial \varepsilon}{\partial x_j}\right] + C_{\varepsilon 1}\frac{\varepsilon}{k}\tau_{ij}\frac{\partial \overline{v}_i}{\partial x_j} - C_{\varepsilon 2}\frac{\varepsilon^2}{k} \qquad i,j = 1,2,3 \text{ in } t \times \Omega \tag{7}$$

in which, the constants $C_u = 0.09$, $C_{\varepsilon 1} = 1.44$, $C_{\varepsilon 2} = 1.92$, and $Pr_t = 1.0$ are found in Launder and Spalding [32] and Wilcox [33], and are considered suitable to an extensive range of turbulent flow conditions [20].

In the solid domain, thermal diffusion is considered the dominant heat transfer mechanism and is modeled in the transient regime [34]:

$$\frac{\partial T}{\partial t} = \alpha_s \frac{\partial^2 T}{\partial x_i^2} \qquad i = 1,2,3 \text{ in } t \times \Omega \tag{8}$$

where T is the temperature, t represents the temporal domain, and α_s refers to the thermal diffusivity of the soil, assumed to be constant. The formulation adopts Einstein's index notation, with the spatial domain Ω described in terms of the spatial dimension x_i, in the direction i.

2.1. Problem description

The problem formulation is illustrated in Fig. 1, which depicts the computational domain of the EAHE-HH system. In Fig. 1a, duct details are presented: the outer diameter of the helical coil (D) is fixed at 0.4 m and the total system length (L) is 3 m; in addition, the internal diameter of the duct (d) is 50 mm. The analysis considers different helical pitch values (P_h), defined in the range of 100 mm to 400 mm, with regular intervals of 50 mm between cases. The variation of P_h, while maintaining a fixed maximum installation length ($L = 3$ m, see Fig. 1a), results in changes to the effective duct length. The vertical distance from the top of the helical coil to the ground surface (L_{sup}) is defined as 1.5 m, yielding a total installation depth (L_T) of 1.9 m ($L_T = L_{sup} + D$). Additionally, the vertical distance from the center of the helical coil to the ground surface is defined by L_c.

As shown in Fig. 1b, the computational domain was established with a soil depth of 15 m, maintaining at least 2 m of spacing between the EAHE-HH duct and the domain boundaries, in accordance with the criteria defined by Rodrigues et al. [35]. The adoption of a 15 m soil depth follows the recommendations of previous studies by Brum et al. [36], Rodrigues et al. [35], and Rodrigues et al. [20]. As demonstrated by Brum et al. [36], beyond this depth the thermal variations induced by the ground-surface boundary condition are no longer significant. This ensures that the domain dimensions do not influence the numerical results. The boundary conditions impose adiabatic behavior on the lateral and bottom surfaces of the soil domain. The thermal conditions at both the ground surface and the duct inlet were defined based on the 2007 climatic data for Viamão, as reported by Vaz et al. [7], and are expressed using the adjusted functions proposed by Brum et al. [36]. These functions, denoted as $T_s(t)$ and $T_{in}(t)$, respectively, are given by:

$$T_s(t) = 291.70 + 6.28 \cdot \sin\left(200.00 \times 10^{-9} t + 26.24\right) \tag{9}$$

$$T_{in}(t) = 296.18 + 6.92 \cdot \sin\left(200.00 \times 10^{-9} t + 26.42\right) \tag{10}$$

As indicated by Vaz et al. [7], the flow conditions assume a constant inlet velocity of 3.3 m/s and a reference manometric pressure of 0 Pa at the outlet. In this study, it is assumed that the airflow is in direct thermal contact with the surrounding soil, following a conceptual perforated-duct approach widely adopted in the literature; under this assumption, the pipe wall is disregarded. Within this framework, the no-slip and impermeability conditions are applied to the air–soil interface. The no-slip condition denotes that the airflow velocity is zero at this interface, which behaves as a solid boundary from a fluid-dynamic standpoint. The impermeability condition, in turn, imposes that no mass transfer occurs between the fluid and the lateral soil surfaces, which in the model correspond to the idealized boundary of the duct. Previous studies have

Table 1
Thermophysical properties of air and soil (Brum et al. [36]).

Properties	Symbol	Air	Soil
Density (kg/m^3)	ρ	1.16	1800
Thermal Conductivity (W/m·K)	k	0.0242	2.1
Specific Heat (J/kg·K)	Cp	1010	1780
Dynamic Viscosity (kg/m·s)	μ	1.798×10^{-5}	–

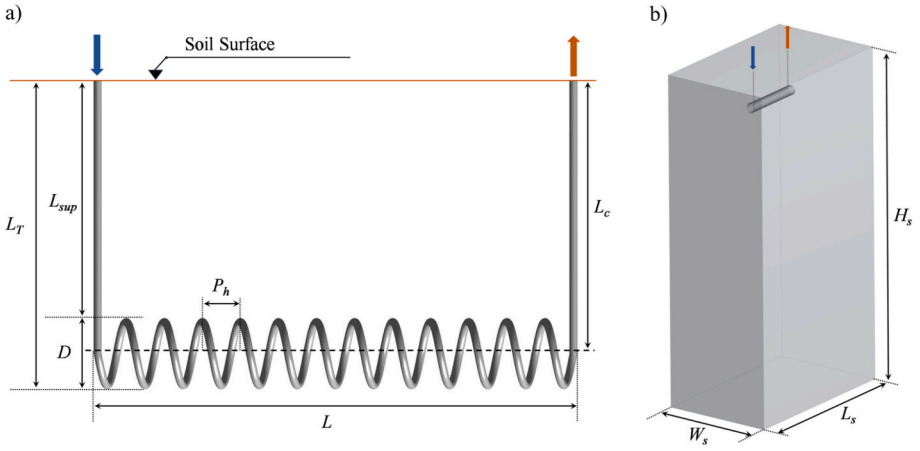

Fig. 1. Geometric configuration of the EAHE-HH system. a) Duct geometry and b) Computational domain layout.

shown that this simplification does not compromise the accuracy of the numerical results [20,37,38]. Table 1 presents the thermophysical properties of air and soil, defined according to the soil characteristics of Viamão and based on the values reported by Brum et al. [36], which was previously verified and validated against the experimental results reported by Vaz et al. [7].

2.2. Performance indicators

The thermal performance of the EAHE-HH will be evaluated through the thermal potential (*TP*) of the system. The *TP* value is determined by the difference in air temperature measured at the entrance and exit of the duct. This parameter can be computed at each time step and is commonly expressed as a mean value over defined periods – daily, monthly, or annual – according to Rodrigues et al. [20]:

$$TP = \frac{1}{n}\sum_{i=1}^{n}\left[T_i^o(t) - T_i^{in}(t)\right] \tag{11}$$

in which $T_i^o(t)$ and $T_i^{in}(t)$ refer to the temperatures of the air at the outlet and inlet sections of the EAHE, in that order, measured at each time period t, based on a set of n recorded data. This performance indicator needs to be maximized.

For the fluid dynamics assessment, the pressure drop (*PD*) within the duct of the EAHE-HH is used as a performance indicator, defined [20]:

$$PD = P_{in} - P_o \tag{12}$$

where P_{in} and P_o denote the mean pressures, respectively, on the inlet face and outlet face of the duct. Unlike *TP*, the *PD* value must be minimized.

The TOPSIS approach applied in this study, customized for the evaluation of EAHE systems, follows the methodological procedure described by Andrade et al. [22]. In this context, the *TP* is treated as the beneficial criterion, whereas the *PD* represents the cost criterion. The TOPSIS approach allows assigning distinct weights to the benefit and cost criteria to reflect their relative importance in the evaluation. In this study, w_1 and w_2 correspond to the weights attributed to thermal and fluid dynamic relevance, respectively, subject to the condition that their sum equals unity ($w_1 + w_2 = 1$). From this, for each geometric configuration, the *TP* and *PD* values are first normalized and subsequently weighted according to w_1 and w_2. In this framework, the weighted normalized values of *TP* and *PD* are used to define the positive ideal solution (corresponding to the maximum *TP* and minimum *PD*) and the negative ideal solution (minimum *TP* and maximum *PD*). For each geometric configuration, the Euclidean distances to these two reference solutions are then calculated. These distances, denoted as S_i^+ and S_i^-, quantify how far each alternative lies from the positive and negative ideal solutions, respectively, within the weighted normalized criterion space.

The performance indicator C_i proposed by Hwang and Yoon (1981) is then calculated directly from these distances as:

$$C_i = \frac{S_i^-}{\left(S_i^+ + S_i^-\right)}, 0 < C_i < 1 \tag{13}$$

Therefore, alternatives that are closer to S_i^+ and farther from S_i^- yield higher C_i values and, consequently, achieve superior rankings in the multi-objective evaluation, with C_i ranging between 0 and 1. In this way, C_i integrates the contributions of *TP* and *PD* into a single metric, enabling a coherent and technically consistent comparison among the geometric alternatives. For a more detailed presentation of the TOPSIS procedure as applied specifically to EAHE systems, the works of Andrade et al. [22] and Razera et al. [19] provide detailed formulations and implementations tailored to this class of thermal–fluid problems. The general mathematical foundations of the method are presented by Hwang and Yoon [26].

3. Numerical modeling

The numerical model employed in the present study is based on the works of Rodrigues et al. [20] and Vaz et al. [16]. The geometric construction was developed using *Design Modeler*, while the spatial discretization was carried out in *MESH*, both tools available in the ANSYS® software package. The solutions were obtained using FLUENT® (version 2024 R2) which is based on the Finite Volume Method (FVM) [39–41]. Separate numerical simulations were performed to address the thermal and fluid dynamic behaviors of the system. The fluid dynamic analysis was restricted to the internal airflow within the EAHE duct (Fig. 1a), whereas the thermal analysis incorporated the interaction between the duct and the soil domain (Fig. 1b).

The thermal simulation was conducted using an unstructured three-dimensional mesh composed of tetrahedral control volumes. The mesh density was set according to the domain: in the surrounding soil region, the characteristic volume size was established as three times the duct diameter ($3d$), while inside the duct, a finer resolution of $d/3$ was applied, as recommended by Rodrigues et al. [20]. The model was solved under unsteady-state conditions using a temporal resolution of $\Delta t = 21{,}600$ s, over a total of 2920 time steps, corresponding to a two-year simulation period. The adoption of this time-step size follows the findings of Rodrigues et al. [20], who demonstrated that time steps equal to or smaller than 21,600 s do not significantly affect the outlet-air temperature or the monthly and annual averages. This choice is further supported by an additional consistency check performed in the present study, which confirmed that reducing the time step to 1800 s yields outlet-temperature results that remain effectively unchanged when compared with those obtained using 21,600 s. To ensure thermal stabilization of the soil, only the data from the second simulated year were used for performance assessment, following the approach described by Brum et al. [36]. In the fluid dynamic analysis, the domain was discretized using finite volumes with dimensions equal to one-sixteenth of the duct diameter ($d/16$), following the approach of Rodrigues et al. [20]. A time step of $\Delta t = 0.1$ s was adopted, and 300 time steps were executed to ensure that the airflow traversed the entire duct at least twice.

The turbulence flow was modeled using the k–ε approach. To discretize the advective terms, a second-order upwind scheme was applied to the momentum equations and similarly extended to the energy equation in the thermal analysis. The coupling for pressure and velocity was handled using the Semi-Implicit Method for Pressure-Linked Equations Consistent (SIMPLE) algorithm. Temporal discretization was based on a second-order implicit formulation, and pressure interpolation also followed a second-order scheme. Additionally, the discretization of terms in the turbulence model equations was carried out using the same second-order Upwind approach. The solution was considered converged once the residuals for both the continuity and momentum equations reached values lower than 10^{-6} for the fluid dynamic problem, and below 10^{-3} for the thermal problem, with the energy equation converging at a residual of 10^{-6}.

The meshes adopted and defined in accordance with previous EAHE studies, as previously mentioned, were subjected to a mesh independence assessment for both the thermal and fluid-dynamic models, with the refinement results summarized in Tables 2 and 3, respectively. For the thermal problem, successive meshes were evaluated based on the

Table 2
Thermal mesh convergence test with tetrahedral volumes.

Mesh Refinement			
Duct	Soil	T_o (6.3072 × 10^7 s)	$100\cdot\left\lvert\frac{T_o^j - T_o^{j+1}}{T_o^{j+1}}\right\rvert$
$d/2$	$4 \times d$	22.848	2.835
$d/3$	$3 \times d$	22.218	0.091
$d/4$	$2 \times d$	22.239	

Table 3
Fluid-dynamic mesh convergence test with hexahedral volumes.

Mesh Refinement	P_{in}	P_o	PD	$100\cdot\left\|\frac{PD^j - PD^{j+1}}{PD^{j+1}}\right\|$
$d/6$	7.584	141.871	134.287	8.996
$d/10$	7.670	130.873	123.203	1.032
$d/13$	7.758	129.703	121.945	0.071
$d/16$	7.770	129.627	121.858	0.639
$d/18$	7.854	130.496	122.642	–

outlet-air temperature at the end of the two-year simulation (6.3072×10^7 s), whereas for the fluid-dynamic problem the pressure drop along the duct was used as the reference quantity. In this procedure, the indices j and $j + 1$ denote, respectively, the mesh under evaluation and the subsequent refinement level, allowing a systematic comparison across discretization levels.

For the thermal analysis, the difference between the adopted mesh and the mesh with finest refinement level was below 0.091 %, while the corresponding deviation in pressure drop remained under 0.64 %. Variations of this magnitude fall within the range typically accepted for EAHE numerical simulations, as reported in Rodrigues et al. [20] and Rodrigues et al. [35], confirming that the selected meshes provide stable and grid-independent results.

3.1. Thermal model verification

To verify the thermal computational model, a simulation was conducted for the Vertical Helical Earth–Air Heat Exchanger (EAHE-VH) studied by Vaz et al. [16], which had previously been verified and validated based on the work of Vaz et al. [7]. This system exhibits thermal and fluid dynamic characteristics similar to those investigated in the present study. The numerically modeled system consists of a cylindrical soil domain with a surface diameter of 4.4 m and a depth of 15 m. The EAHE-VH features a helical diameter of 0.4 m, a vertical length of 3 m, a duct diameter of 50 mm, and a vertical pitch of 100 mm between helicoids. The thermophysical properties of the air and soil, as well as the boundary conditions, were consistent with those adopted in the present analysis. Fig. 2 presents the temperature distribution based on daily average values at the outlet section of the EAHE, comparing the current results with those obtained by Vaz et al. [16], and demonstrating good agreement between the models. The percentage relative difference (RD(%)) between the results was calculated using:

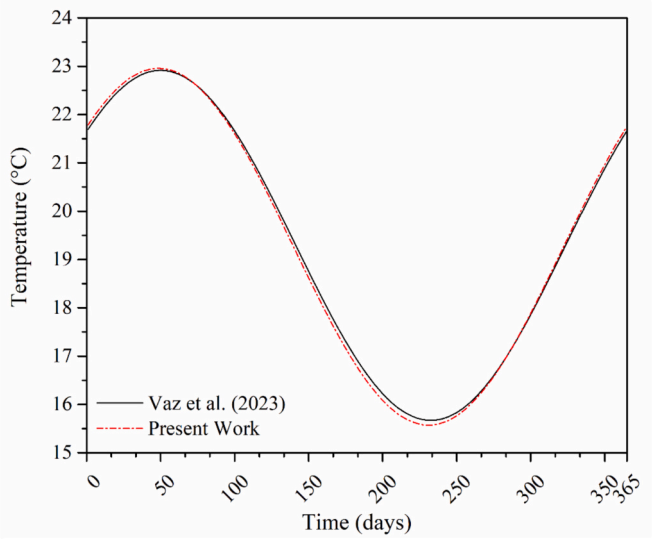

Fig. 2. Verification of the thermal numerical model based on daily average air temperature from the present study compared to results from Vaz et al. [16].

$$RD(\%) = 100\cdot\left|\frac{\overline{T_o^{Est}}^D - \overline{T_o^{Ref}}^D}{\overline{T_o^{Est}}^D}\right| \tag{14}$$

where $\overline{T_o^{Est}}^D$ represents the temperature from the present simulation and $\overline{T_o^{Ref}}^D$ denotes the reference temperature. Based on the RD(%) calculation, the maximum percentage relative difference observed in daily average outlet temperatures over the course of one year was 0.88 % (0.15 °C). In Table 4, a monthly comparative analysis was conducted using two quantitative indicators: the Root Mean Square Error (RMSE) and the Mean Absolute Percentage Error (MAPE) [42]. These metrics were calculated between the numerical predictions and the reference dataset used for verification. The results demonstrated consistently low RMSE and MAPE values across all months, indicating a high level of agreement. This additional assessment confirms that the thermal behavior predicted by the model remains closely aligned with the reference data on a month-by-month basis. These results demonstrate the effectiveness of the thermal numerical model employed in this study in achieving the intended outputs. This confirms the thermal computational model's applicability in this context and highlights its potential for future investigations, ensuring reliable and accurate predictions.

3.2. Fluid-dynamic model verification

The verification of the fluid dynamic computational model was carried out in two stages. In the first stage, the system's pressure drop was assessed through the analytical formulation presented by Pritchard and Mitchell [43]. The analysis considered a rectilinear duct with a circular cross-section, having an equivalent diameter of 0.05 m – matching the diameter of the EAHE-HH system – and a total length of 30 m. The pressure drop analytical solution proposed by Pritchard and Mitchell [43] is given by:

$$\Delta P_A = PD_A = f\cdot\frac{L_d}{d}\cdot\frac{\rho v^2}{2} \tag{15}$$

where, L_d denotes the duct length ($L_d = 30$ m) and f is the friction factor, defined as [43]:

$$f = \left\{ -1.8\log\left[\left(\frac{\varepsilon/d}{3.7}\right)^{1.11} + \frac{6.9}{Re_d}\right]\right\}^{-2} \tag{16}$$

Within this formulation, ε denotes the duct's relative roughness, and Re_d corresponds to the Reynolds number [44]:

$$Re_d = \frac{\rho\cdot v\cdot d}{\mu} \tag{17}$$

In the second stage of the verification, a regular helical duct was

Table 4
Monthly RMSE and MAPE values used for thermal model verification.

Month	RMSE (°C) $\sqrt{\frac{1}{n}\sum_{i=1}^{n}\left(T_i^{Est} - T_i^{Ref}\right)^2}$	MAPE (%) $\frac{1}{n}\sum_{i=1}^{n}\left\|\frac{T_i^{Ref} - T_i^{Est}}{T_i^{Ref}}\right\|100$
January	0.083	0.373
February	0.049	0.205
March	0.019	0.027
April	0.068	0.310
May	0.117	0.596
June	0.144	0.809
July	0.140	0.853
August	0.106	0.669
September	0.054	0.320
October	0.018	0.043
November	0.058	0.300
December	0.084	−0.395

evaluated, maintaining the same geometric characteristics as the used in the EAHE-HH system. The analysis was based on the correlations proposed by Ali [45], which describes the pressure drop in regular helical pipes and are suitable for the geometric and flow conditions of the present study ($D = 0.4$ m; $L = 3$ m; $d = 0.05$ m and $Re_d = 10{,}696.32$), given by [45]:

$$Eu \cdot G_{rhc} = 0.09 \cdot Re_d^{-1/5}, Re_d > 10,000 \tag{18}$$

where Eu is the Euler number and G_{rhc} is the geometrical number for regular-helical coil, provided, respectively, by [45]:

$$Eu = \frac{PD_C}{2 \cdot \rho \cdot v^2} \tag{19}$$

$$G_{rhc} = d^{0.85} \cdot D_{eq}^{0.15} \cdot L_c^{-1/2} \tag{20}$$

in Eq. (19), PD_C represents the pressure drop obtained from the correlation; and in Eq. (20), the parameter D_{eq} refers to the equivalent diameter of the helical duct, defined as follows [45]:

$$D_{eq} = \frac{\sqrt{P_h^2 + (\pi D)^2}}{\pi} \tag{21}$$

As a result of the fluid dynamic computational model verification, a satisfactory agreement between the numerical and reference solutions was achieved. For the rectilinear duct, the numerical results obtained in the present study ($PD = 117.62$ Pa) showed a maximum relative deviation of approximately 2.3 % when compared to the analytical formulation ($PD_A = 114.90$ Pa) proposed by Pritchard and Mitchell [43]. In the case of the regular helical duct, a relative deviation of approximately 3.1 % was observed, considering the results of present work ($PD = 101.06$ Pa), for $P_h = 200$ mm ($L_d = 18.84$ m), in comparison with the results obtained using the correlation proposed by Ali [45] ($PD_C = 97.91$ Pa). These findings confirm the consistency of the mathematical and numerical models adopted in this study (for both thermal and fluid dynamic simulations), demonstrating its suitability for solving the proposed problem and reinforcing its applicability within the scope of the present work.

4. Results

The thermal and fluid dynamic performance of the system was evaluated through numerical simulations involving multiple configurations of the Horizontal Helical Earth-Air Heat Exchanger (EAHE-HH), in which the helical pitch (P_h) was varied as the geometric parameter. The simulations incorporated temporal temperature fluctuations and the geotechnical characteristics specific to Viamão. The analysis was conducted over a 365-day period, representing an entire climatic year.

4.1. Thermal analyses

Fig. 3 shows the thermal behavior of the EAHE-HH systems through the curves of daily average temperatures obtained at the inlet (T_{in}) and outlet (T_o) of the devices. It can be observed that the different geometric configurations of the EAHE-HH demonstrate effective performance in cooling the air during hot periods (considered as periods when $T_{in} > 25.5$ °C, which defines the upper limit of the reference temperature for summer thermal comfort, according to ABNT NBR 16401-2 [46] and ASHRAE [47]). Under this condition, the outlet temperature (T_o) remains below the inlet temperature curve (T_{in}), reflecting the system's ability to dissipate thermal energy from the air. In contrast, under cold weather conditions ($T_{in} < 21.5$ °C, the lower limit of the reference temperature for winter thermal comfort, according to ABNT NBR 16401-2 [46] and ASHRAE [47]), the system shows a negligible heating capacity, with the outlet temperature curve (T_o) remaining below or slightly above the inlet temperature curve (T_{in}). This behavioral pattern is observed for all P_h values studied.

Fig. 4 presents the temperature field of the EAHE-HH system (for $P_h = 400$ mm) and the surrounding soil, considering: a) a typical summer day (12/31/2007), and b) a typical winter day (07/24/2007). It can be observed that during typical summer periods (Fig. 4a), the installation depth adopted for the EAHE-HH provides a favorable thermal condition

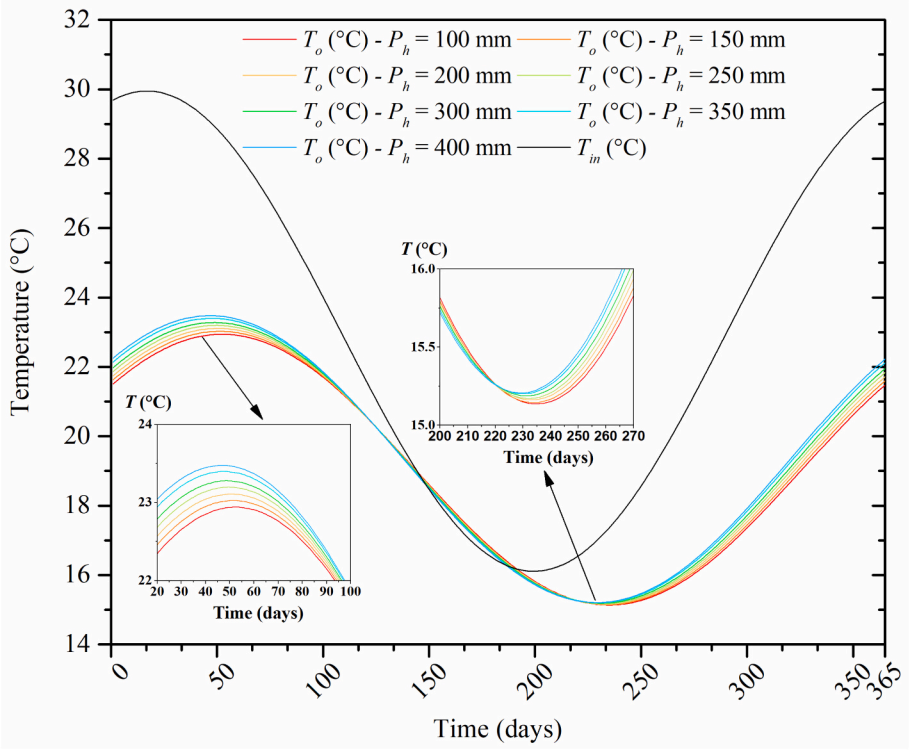

Fig. 3. Thermal behavior of the air based on the inlet (T_{in}) and outlet (T_o) temperatures obtained in the EAHE-HH systems.

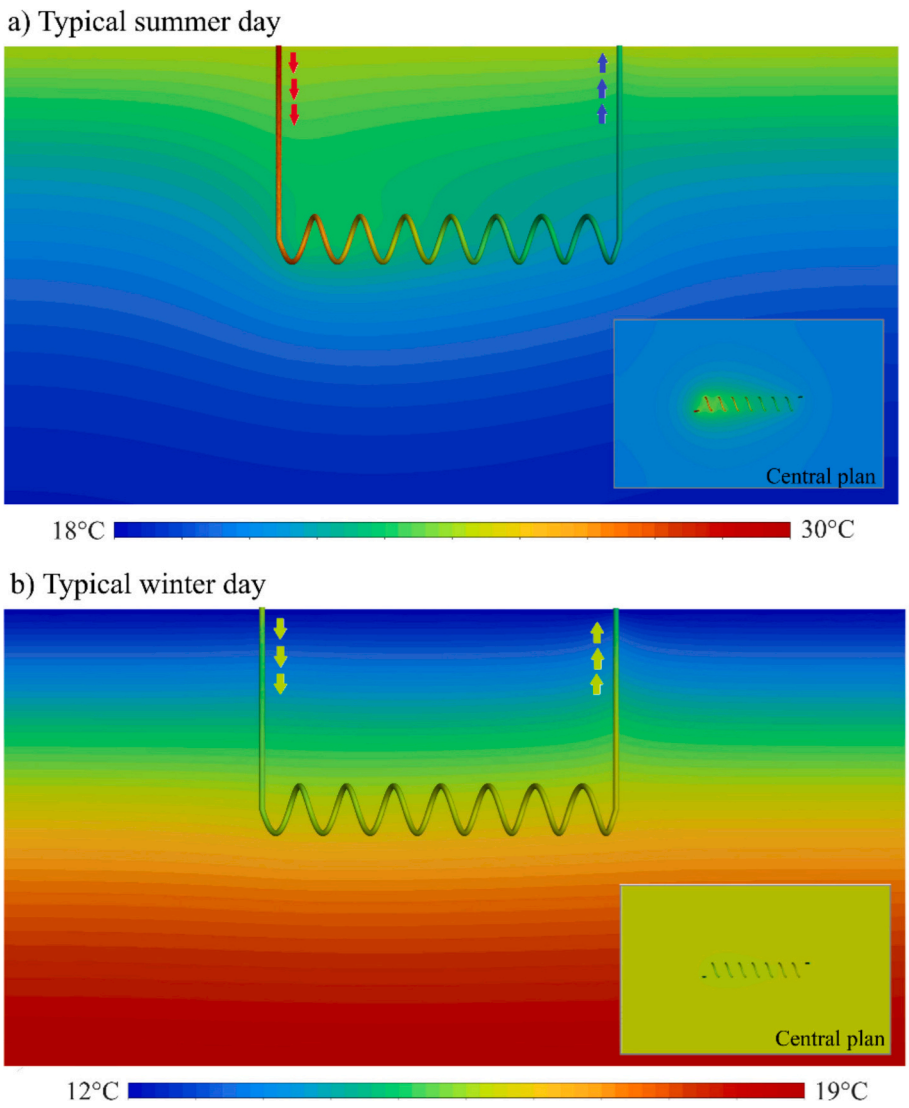

Fig. 4. Temperature field for the EAHE-HH with P_h = 400 mm, for: a) Typical summer day (12/31/2007), and b) Typical winter day (07/24/2007).

for heat exchange between the soil and the air. In this scenario, the air enters the EAHE-HH with an inlet temperature of T_{in} = 29.67 °C, while the central plane of the soil in the region of the EAHE-HH exhibits an approximate average temperature of $T_{S,CP}$ = 21 °C. This temperature difference indicates a significant potential for heat transfer between the two media (EAHE-HH and the portion of soil in which it is embedded). As a result, the air is cooled and exits the device at T_o = 21.49 °C, which is below the recommended thermal comfort temperature range (ABNT NBR 16401-2 [46] and ASHRAE [47]) for summer, defined between 22.5 °C and 25.5 °C, indicating high cooling capacity of the system.

Conversely, on typical winter days (Fig. 4b), the thermal gradient between the inlet air temperature (T_{in}) and the soil in which the EAHE-HH is installed is minimal, indicating low potential for heat transfer between the soil and the air. In this scenario, the air enters the EAHE with a temperature of T_{in} = 16.14 °C, while the central plane of the surrounding soil has an average temperature of $T_{S,CP}$ = 16.17 °C. Consequently, the outlet air temperature shows no significant change in relation to the inlet, resulting in an outlet temperature of T_o = 15.55 °C. In this case, achieving heating potential would require installing the EAHE-HH at a greater depth. It is important to note, however, that even with deeper installation, heating gains would likely remain limited. This is because the maximum soil temperature reached was approximately 19 °C, which suggests that the recommended winter thermal comfort temperature (21 °C to 23.5 °C, according to ABNT NBR 16401-2 [46] and ASHRAE [47]) would likely not be achieved. This behavior is consistent with the observations of Brum et al. [36], who investigated the effect of installation depth of Horizontal Rectilinear EAHE (EAHE-HR) under the same climatic and soil conditions.

Fig. 5 illustrates the monthly average thermal potential ($\overline{TP}^M$) of the EAHE-HH for the different P_h values, as well as the monthly average inlet ($\overline{T_{in}}^M$) and outlet ($\overline{T_o}^M$) air temperatures in the EAHE-HH. During hot periods ($\overline{T_{in}}^M > 25.5$ °C – January, February, March, November, and December), the system demonstrates a high air cooling capacity for all P_h values, providing outlet air temperatures within or even below the thermal comfort limits $\overline{T_o}^M$. Conversely, during cold periods ($\overline{T_{in}}^M <$ 21.5 °C, May, June, July, August, and September), only the month of June shows a minimal heating condition. For the remaining months (May, June, August, and September), a slight cooling condition is observed, making the system unsuitable for operation during these periods and highlighting its limited capacity for air heating. Finally, in April and October, $\overline{T_{in}}^M$ already falls within the recommended thermal comfort range, making the use of the system unnecessary during these months. Additionally, it is observed that increasing P_h within the range of 100 mm $\leq P_h \leq$ 400 mm results in a gradual reduction in the system's cooling performance. Among the tested configurations, the EAHE-HH

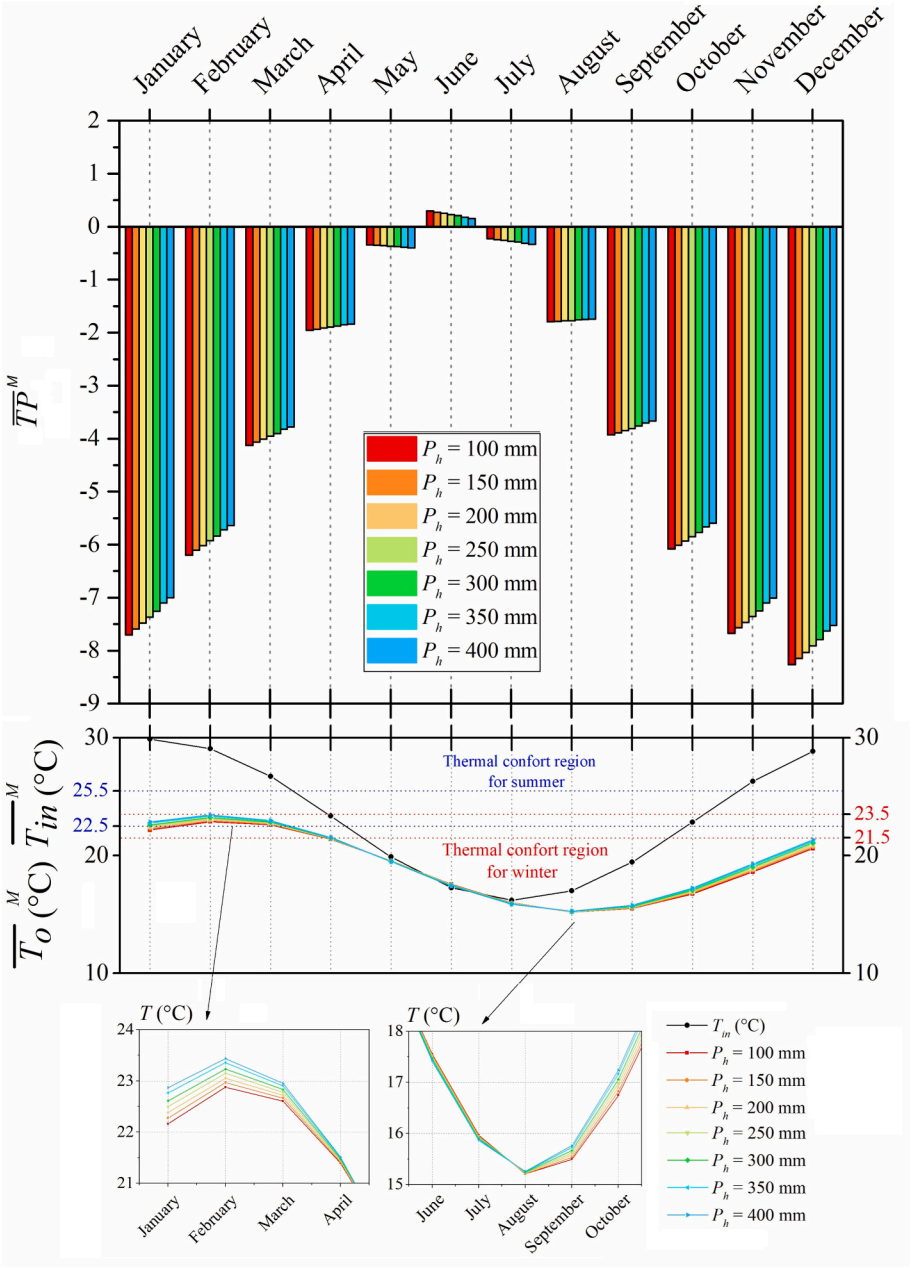

Fig. 5. Monthly thermal assessment of the EAHE-HH under different P_h configurations.

with a helical pitch of 100 mm demonstrated superior average thermal performance, being up to 10.07 % more effective in January when compared to the EAHE-HH with P_h = 400 mm, which presented the poorest performance in terms of $\overline{TP}^M$. However, it is important to highlight that the EAHE-HH with P_h = 400 mm still fulfills the objective of air temperature reduction and, due to its simpler construction compared to the other configurations, it can be considered a viable alternative for thermal conditioning.

Fig. 6 provides further insight into this behavior. As previously discussed, the EAHE-HH with P_h = 100 mm exhibited the greatest cooling effectiveness among the evaluated configurations. This effect is explained by the temperature distribution along the duct: for P_h = 100 mm, heat transfer is more pronounced in the first two-thirds of the EAHE-HH length, already achieving thermal comfort conditions within this section (see Fig. 6a). However, in the final third, the heat transfer decreases significantly due to the reduced temperature gradients between the soil and the circulating air. This suggests that the P_h = 100 mm configuration can deliver effective thermal performance even with shorter duct lengths, making it a promising option for buildings with limited space available for EAHE installation, in other words, a potential solution for even more compact EAHE-HH systems. On the other hand, the geometry with P_h = 400 mm requires the air to flow through the entire length of the helical EAHE (L) for the thermal comfort condition to be achieved (see Fig. 6b). Although it presents lower heat transfer along the duct, this configuration satisfactorily fulfills the cooling function. Furthermore, since it requires a shorter duct length compared to the other configurations, it results in lower material consumption, which implies cost reduction and greater construction simplicity, thus representing a viable alternative.

Fig. 7 compares the performance of the EAHE-HH with P_h = 100 mm – which exhibited the most favorable thermal potential among the configurations analyzed – with numerical results from other EAHE designs: the Horizontal Rectilinear EAHE (EAHE-HR) and the Vertical Helical EAHE (EAHE-VH, P_h = 100 mm), presented by Vaz et al. [16],

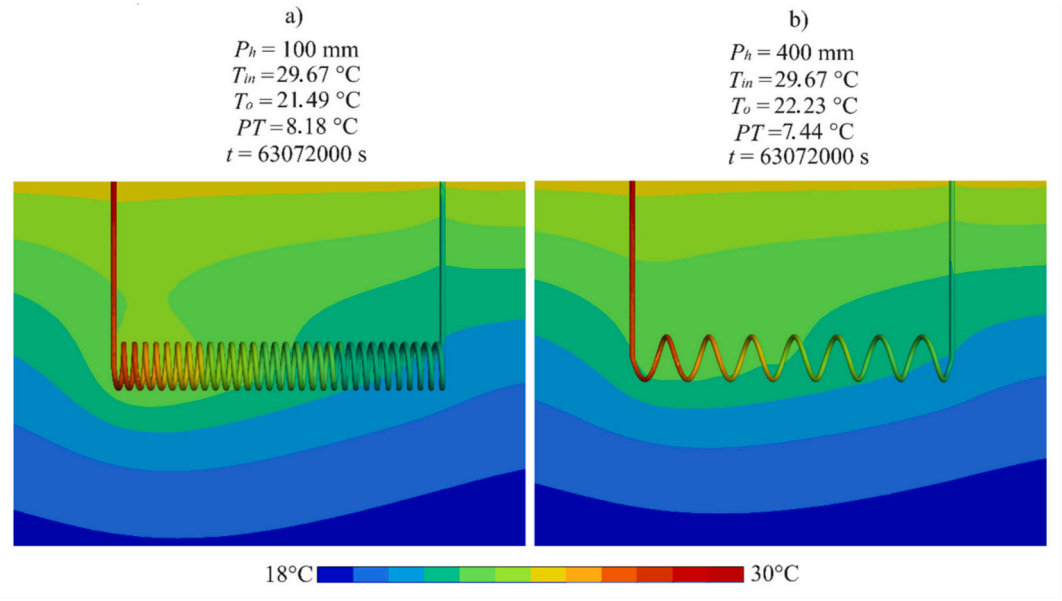

Fig. 6. Temperature distribution for the EAHE-HH, considering: a) P_h = 100 mm and b) P_h = 400 mm.

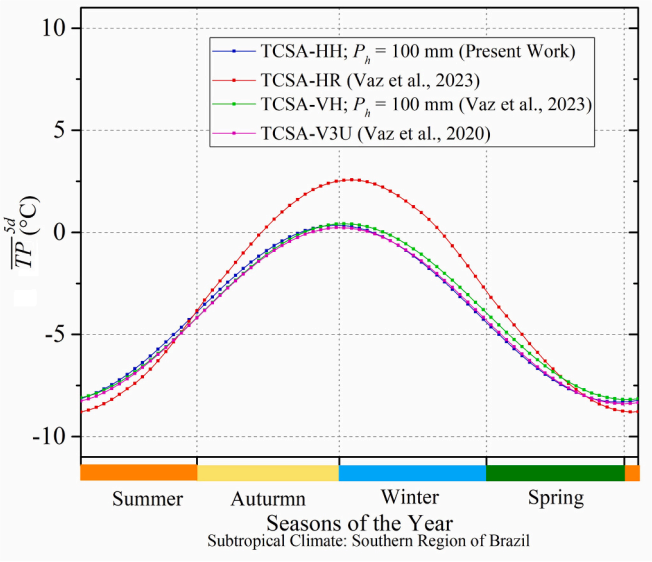

Fig. 7. Thermal performance of the EAHE-HH (P_h = 100 mm) compared to other EAHE geometric configurations under the climate and soil conditions of Viamão.

and the Vertical EAHE with 3 U-shaped ducts (EAHE-V3U), presented by Vaz et al. [13]. The comparison was based on the thermal potential averaged over five days ($\overline{TP}^{5d}$). All systems were evaluated under identical soil and climate conditions for the city of Viamão. Overall, the response curves for the different EAHE designs exhibit similar behavior, with particular emphasis on the EAHE-HR, which demonstrated air heating capacity during colder periods. Regarding the cooling performance, all configurations showed relevant thermal behavior. In terms of magnitude, the EAHE-HH (P_h = 100 mm) delivered satisfactory cooling results when compared to the other evaluated geometries. Specifically, considering the average cooling thermal potential during the summer and spring periods, the EAHE-HH outperformed the EAHE-VH by 1.66 %. In contrast, it exhibited slightly lower performance if compared to the EAHE-HR and EAHE-V3U, with differences of 0.48 % and 1.30 %, respectively.

Based on these results, one can observe that the performance difference among the distinct geometric configurations under cooling conditions was practically negligible. In this context, factors such as the available land area and the soil drilling conditions become decisive criteria in selecting the most appropriate EAHE for each application, with preference given to solutions that require shallower depths and smaller surface areas. The EAHE-HR, as analyzed by Vaz et al. [16], requires a significant surface extension of 25.77 m and is installed at a depth of 3.0 m. Despite these demands, it was the only system capable of promoting air heating during colder periods, in addition to achieving the best cooling performance during the hotter months. As an alternative, the EAHE-HH operates at a shallower depth of 1.9 m and requires only 3.0 m of surface extension, representing a more compact solution with reduced drilling requirements. The EAHE-VH, in turn, stands out for its minimal surface area requirement (0.4 m), although it also requires an installation depth of 3.0 m. Finally, the EAHE-V3U is designed to operate at a depth of 3.0 m with a surface extension of 3.2 m, with its main advantage being the simpler construction compared to the helical configurations.

4.2. Fluid dynamics analyses

The objective of the fluid dynamic analysis was to evaluate the pressure difference between the inlet and outlet of the EAHE-HH system, with the aim of minimizing the power consumption of the ventilation unit. Fig. 8 presents the fluid dynamic behavior of the EAHE-HH as a function of the pressure drop (*PD*) indicator and the total duct length (L_d). As expected, increasing the horizontal pitch (P_h) led to a progressive reduction in *PD* values. This trend is associated with the fact that larger spacing between the helical turns results in a shorter total duct length (L_d), which directly contributes to a reduction in overall pressure losses (*PD*). Among the configurations analyzed, the case with P_h = 400 mm yielded the lowest pressure drop, representing a reduction of 66.81 % in *PD* when compared to the configuration with P_h = 100 mm, which exhibited the highest *PD*. Therefore, although reducing the P_h enhances the cooling performance of the system, it also results in a disadvantage concerning fluid dynamic behavior. Smaller P_h values lead to increased pressure drop, requiring higher operational demand from the ventilation system and, consequently, resulting in higher energy consumption.

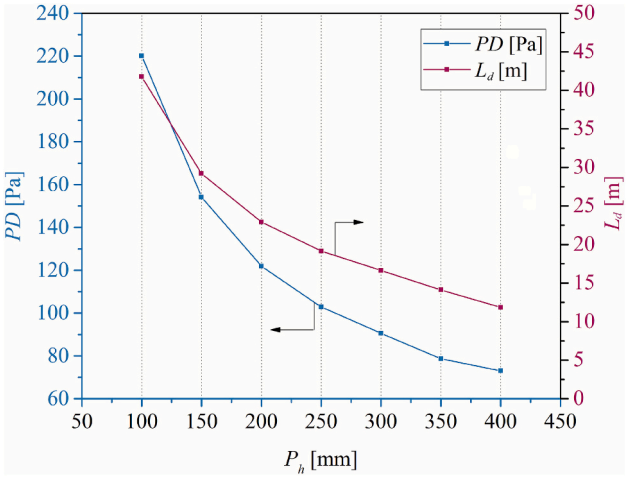

Fig. 8. Influence of helical pitch (P_h) on pressure drop (PD) and duct length (L_d) in the EAHE-HH system.

4.3. Multi-objective performance analysis (TOPSIS)

Finally, Fig. 9 presents the multiobjective analysis of the EAHE-HH, which simultaneously considers the thermal performance and pressure drop as evaluation criteria. The evaluation was performed using the C_i metric as a measure of overall performance, obtained through the TOPSIS method and defined by Eq. (13). To ensure a comprehensive assessment of the multi-objective behavior of the EAHE-HH, the TOPSIS evaluation was performed over a wide range of weight combinations, with w_1 and w_2 systematically varied under the constraint $w_1 + w_2 = 1$. This procedure allows the analysis to characterize the full spectrum of relative influences between thermal potential (TP) and pressure drop (PD). For the thermal performance indicator, the Absolute Average Thermal Potential $|\overline{TP}|$was adopted, calculated for the months of January, February, November, and December, which correspond to the periods with the highest average values of thermal potential obtained in the analysis. When the fluid dynamic criterion exerts greater influence than the thermal criterion ($w_1 < w_2$, lower region of the graph), the highest C_i values are observed for geometries with P_h values between 300 and 400 mm. Notably, the configuration with $P_h = 400$ mm achieved the best performance in all where the fluid dynamic criterion was prioritized over the thermal objective, thus representing the most suitable solution under such conditions. Even as the weight shifts in favor of the thermal aspect, this configuration continues to perform favorably in the multiobjective analysis. This behavior highlights the robustness and stability of these configurations with respect to the thermal (TP) and fluid dynamic (PD) performance indicators, even in scenarios where the thermal criterion accounts for up to 75 % of the weighting ($w_1 = 0.75$; $w_2 = 0.25$). This pattern suggests that geometric variations of the EAHE-HH, through changes in P_h, have a more significant impact on the system's fluid dynamic aspects.

Nevertheless, with the growing predominance of the thermal criterion, a clear shift in optimal configurations can be observed. Accordingly, for thermal relevance levels between 55 % and 70 %, the geometry with $P_h = 350$ mm emerges as the most suitable configuration. As thermal relevance increases to the range of 75 % to 85 %, the configuration with $P_h = 300$ mm demonstrates superior performance. For even higher thermal priorities, a progressive reduction in the helical pitch becomes favorable: $P_h = 250$ mm is identified as the best choice at 90 % thermal relevance, while $P_h = 150$ mm and $P_h = 100$ mm are the most effective configurations for 95 % and 99 %, respectively. These findings reinforce the system's adaptability and underscore the importance of aligning geometric configurations with the intended balance between thermal and fluid dynamic performance goals.

5. Conclusions

Based on the results obtained, it can be concluded that the different geometric configurations of the horizontal helical earth-air heat

PD w_2	$\|\overline{TP}\|$ w_1	P_h (mm) 100	150	200	250	300	350	400
0.01	0.99	**0.8910**	0.8290	0.6834	0.5237	0.3749	0.1786	0.1090
0.05	0.95	0.6107	**0.6966**	0.6790	0.5937	0.5117	0.4238	0.3893
0.10	0.90	0.4263	0.5764	0.6735	**0.6834**	0.6546	0.6030	0.5737
0.15	0.85	0.3187	0.5169	0.6708	0.7336	**0.7372**	0.7056	0.6813
0.20	0.80	0.2483	0.4873	0.6695	0.7601	**0.7867**	0.7715	0.7517
0.25	0.75	0.1985	0.4716	0.6689	0.7746	**0.8179**	0.8171	0.8015
0.30	0.70	0.1615	0.4629	0.6685	0.7829	0.8382	**0.8504**	0.8385
0.35	0.65	0.1329	0.4576	0.6683	0.7879	0.8517	**0.8756**	0.8671
0.40	0.60	0.1102	0.4544	0.6682	0.7911	0.8609	**0.8951**	0.8898
0.45	0.55	0.0917	0.4523	0.6681	0.7931	0.8671	**0.9106**	0.9083
0.50	0.50	0.0763	0.4509	0.6681	0.7945	0.8715	0.9229	**0.9237**
0.55	0.45	0.0633	0.4500	0.6681	0.7954	0.8745	0.9327	**0.9367**
0.60	0.40	0.0522	0.4493	0.6680	0.7960	0.8767	0.9406	**0.9478**
0.65	0.35	0.0426	0.4489	0.6680	0.7965	0.8782	0.9468	**0.9574**
0.70	0.30	0.0342	0.4486	0.6680	0.7968	0.8792	0.9517	**0.9658**
0.75	0.25	0.0268	0.4484	0.6680	0.7970	0.8799	0.9553	**0.9732**
0.80	0.20	0.0202	0.4482	0.6680	0.7971	0.8804	0.9580	**0.9798**
0.85	0.15	0.0144	0.4481	0.6680	0.7972	0.8807	0.9598	**0.9856**
0.90	0.10	0.0091	0.4481	0.6680	0.7973	0.8809	0.9609	**0.9909**
0.95	0.05	0.0043	0.4480	0.6680	0.7973	0.8810	0.9615	**0.9957**
0.99	0.01	0.0008	0.4480	0.6680	0.7973	0.8811	0.9617	**0.9992**

Fig. 9. Multiobjective performance: C_i values according to P_h considering various weight distributions between thermal (w_1) and fluid dynamic (w_2) criteria.

exchangers (EAHE-HH), evaluated through the variation of P_h, demonstrated significant performance in air cooling during hot periods, effectively achieving the desired thermal comfort condition. However, the system's heating capability was negligible during cold periods. Therefore, to achieve a heating potential, the EAHE-HH would need to be installed at a greater depth. Even so, the heating gains would remain minimal for the location and climatic conditions assessed. Specifically, during the months of January, February, March, November, and December, the EAHE-HH performed adequately for air cooling. In contrast, during the remaining months, the use of the system proved unnecessary.

It was also observed that increasing P_h led to a reduction in the thermal response, with the EAHE-HH configuration using $P_h = 100$ mm showing the highest average thermal performance. On the other hand, the configuration with $P_h = 400$ mm exhibited the lowest average thermal performance, although it still achieved the desired cooling effect. When comparing these results with data available in the literature, it was found that the EAHE-HH achieved a cooling performance similar to other EAHE models installed in the same region, making it a viable alternative for compact plots or scenarios requiring minimal ground excavation. Thus, the EAHE-HH stands out as a promising solution for air cooling during hot periods, despite its limitations in colder months. As expected, increasing the horizontal pitch (P_h) led to a progressive reduction in pressure drop (*PD*) values. Among the configurations analyzed, the case with $P_h = 400$ mm yielded the lowest pressure drop, representing a 66.81 % reduction compared to the configuration with $P_h = 100$ mm, which exhibited the highest *PD*.

The TOPSIS method proved effective in multiobjective evaluating the performance indicators *TP* and *PD*, identifying the best-performing configurations. The geometry with $P_h = 400$ mm achieved the best performance in all scenarios where the fluid dynamic criterion was prioritized over the thermal objective, including when both criteria were equally weighted. For cases with increasingly dominant thermal criteria, a progressive reduction in helical pitch became favorable: $P_h = 250$ mm was identified as best at 90 % thermal relevance, while $P_h = 150$ mm and $P_h = 100$ mm were the most effective configurations at 95 % and 99 %, respectively. From a broader design standpoint, the configuration with $P_h = 400$ mm demonstrates the most robust overall behavior, consistently meeting the cooling comfort criterion while maintaining stable performance across different weighting scenarios. Thus, $P_h = 400$ mm stands out as the most practical and broadly applicable choice for design purposes.

Future research could expand the current findings by exploring new configurations and operating conditions of the EAHE-HH system. In particular, numerical simulations could be conducted in different climatic and soil conditions, installation depths, and duct cross-sectional geometries, in order to assess the performance and adaptability of the system across diverse scenarios. The integration of optimization techniques and cost–benefit analyses could also contribute to the practical implementation of EAHE-HH solutions on a broader scale.

CRediT authorship contribution statement

Andre L. Razera: Writing – original draft, Visualization, Validation, Software, Methodology, Investigation, Data curation. **Cesare Biserni:** Writing – review & editing, Funding acquisition, Formal analysis. **Michel K. Rodrigues:** Writing – original draft, Visualization, Validation, Software, Methodology, Investigation, Formal analysis, Data curation. **Luiz A.O. Rocha:** Writing – review & editing, Supervision, Resources, Project administration, Investigation, Funding acquisition, Formal analysis, Conceptualization. **Elizaldo D. dos Santos:** Writing – review & editing, Supervision, Resources, Project administration, Investigation, Funding acquisition, Formal analysis, Data curation, Conceptualization. **Liércio A. Isoldi:** Writing – review & editing, Writing – original draft, Visualization, Validation, Supervision, Software, Methodology, Investigation, Funding acquisition, Formal analysis, Data curation, Conceptualization.

Declaration of competing interest

The authors declare that they have no known competing financial interests or personal relationships that could have appeared to influence the work reported in this paper.

Acknowledgments

The authors gratefully acknowledge the Conselho Nacional de Desenvolvimento Científico e Tecnológico (CNPq), under grant numbers 150193/2023-8, 307791/2019-0, 308396/2021-9, and 309648/2021-1, for their research scholarships. The authors also acknowledge the Fundação de Amparo à Pesquisa do Estado do Rio Grande do Sul (FAPERGS) for financial support, under grant numbers 23/2551-0000165-9, 21/2551-0002231-0, and 19/2551-0000165-9.

Data availability

Data will be made available on request.

References

[1] K.K. Agrawal, R. Misra, G.D. Agrawal, M. Bhardwaj, D.K. Jamuwa, Effect of different design aspects of pipe for earth air tunnel heat exchanger system: a state of art, Int. J. Green Energy 16 (8) (2019) 598–614, https://doi.org/10.1080/15435075.2019.1601096.

[2] Koshlak., A review of earth-air heat exchangers: from fundamental principles to hybrid systems with renewable energy integration, Energies 18 (5) (2025) 1017, https://doi.org/10.3390/en18051017.

[3] Z. Liu, M. Xie, Y. Zhou, Y. He, L. Zhang, G. Zhang, D. Chen, A state-of-the-art review on shallow geothermal ventilation systems with thermal performance enhancement system classifications, advanced technologies and applications, Energy Built Environ. 4 (2) (2023) 148–168, https://doi.org/10.1016/j.enbenv.2021.10.003.

[4] S.F. Ahmed, M.M.K. Khan, M.T.O. Amanullah, M.G. Rasul, N.M.S. Hassan, A parametric analysis of the cooling performance of vertical earth-air heat exchanger in a subtropical climate, Renew. Energy 172 (2021) 350–367, https://doi.org/10.1016/j.renene.2021.02.086.

[5] J. Zhao, B. Huang, Y. Li, Y. Zhao, Comprehensive review on climatic feasibility and economic benefits of earth-to-air heat exchanger (EAHE) systems, Sustain Energy Technol Assess 68 (2024) 103862, https://doi.org/10.1016/j.seta.2024.103862.

[6] A.S. Ramadan, Parametric Study of Vertical Ground Loop Heat Exchangers for Ground Source Heat Pump Systems, Ph.D. Thesis,, The University of Western Ontario, Canada, 2016.

[7] J. Vaz, M.A. Sattler, E.D. dos Santos, L.A. Isoldi, Experimental and numerical analysis of an earth–air heat exchanger, Energ. Buildings 43 (9) (2011) 2476–2482, https://doi.org/10.1016/j.enbuild.2011.06.003.

[8] G. Mihalakakou, M. Souliotis, M. Papadaki, G. Halkos, J. Paravantis, S. Makridis, S. Papaefthimiou, Applications of earth-to-air heat exchangers: a holistic review, Renew. Sustain. Energy Rev. 155 (2022) 111921, https://doi.org/10.1016/j.rser.2021.111921.

[9] J. Xiao, J. Li, Influence of different types of pipes on the heat exchange performance of an earth-air heat exchanger (2024), Case Stud. Therm. Eng. 55 (2024) 104116, https://doi.org/10.1016/j.csite.2024.104116.

[10] S.E. Sofyan, T.M.I. Riayatsyah, E. Hu, A. Tamlicha, T.M.R. Pahlefi, H.B. Aditiya, Computational fluid dynamic simulation of earth air heat exchanger: a thermal performance comparison between series and parallel arrangements, Results Eng. 24 (2024) 102932, https://doi.org/10.1016/j.rineng.2024.102932.

[11] Z. Liu, Z.J. Yu, T. Yang, L. Roccamena, P. Sun, S. Li, M. El Mankibi, Numerical modeling and parametric study of a vertical earth-to-air heat exchanger system, Energy 172 (2019) 220–231, https://doi.org/10.1016/j.energy.2019.01.098.

[12] N. Soares, N. Rosa, H. Monteiro, J.J. Costa, Advances in standalone and hybrid earth-air heat exchanger (EAHE) systems for buildings: a review, Energ. Buildings 253 (2021) 111532, https://doi.org/10.1016/j.enbuild.2021.111532.

[13] I.S. Vaz, J. Vaz, L.C. Vitoria, L.A. Rocha, V.D. Hermes, E.D. Santos, M.K. Rodrigues, L.A. Isoldi, Numerical analysis comparing the thermal performance of vertical and horizontal earth-air heat exchangers, in: 18th Brazilian Congress of Thermal Sciences and Engineering, ENCIT 2020, 2020.

[14] A. Mathur, S. Mathur, G.D. Agrawal, J. Mathur, Comparative study of straight and spiral earth air tunnel heat exchanger system operated in cooling and heating modes, Renew. Energy 108 (2017) 474–487, https://doi.org/10.1016/j.renene.2017.03.001.

[15] A. Mathur, S. Kumar, Thermal performance and comfort assessment of U-shape and helical shape earth-air heat exchanger in India, Energy Built Environ. 3 (2) (2022) 171–180, https://doi.org/10.1016/j.enbenv.2021.01.002.

[16] I. Vaz, S. Griebeler, M. Rodrigues, L. Rocha, E. dos Santos, L. Isoldi, Numerical analysis of a vertical helical earth-air heat exchanger, Revista de Engenharia Térmica 22 (2) (2023) 13–19, https://doi.org/10.5380/reterm.v22i2.91757.
[17] F. Taşdelen, İ. Dağtekin, A numerical study on cooling performance of different type earth-air heat exchangers, Renew. Energy 241 (2025) 122325, https://doi.org/10.1016/j.renene.2024.122325.
[18] K. Huang, Q. Sun, G. Feng, L. Zhang, A. Li, J. Wei, X. Meng, Experimental and numerical research on the thermal performance of a vertical earth-to-air heat exchanger system, Geothermics 125 (2025) 103182, https://doi.org/10.1016/j.geothermics.2024.103182.
[19] A.L. Razera, I.S. Vaz, R.J.C.D. Fonseca, M.K. Rodrigues, L.A.O. Rocha, E.D. dos Santos, L.A. Isoldi, Multiobjective numerical analysis of thermal and fluid dynamics performance of a vertical helical earth–air heat exchanger using the TOPSIS method, Heat Transfer. (2025), https://doi.org/10.1002/htj.70022.
[20] M.K. Rodrigues, J. Vaz, L.A.O. Rocha, E.D. dos Santos, L.A. Isoldi, A full approach to earth-air heat exchanger employing computational modeling, performance analysis and geometric evaluation, Renew. Energy 191 (2022) 535–556, https://doi.org/10.1016/j.renene.2022.04.007.
[21] J. Xiao, Y. Hu, Q. Wang, J. Li, Structural design method, validation, and performance analysis of an earth-air heat exchanger for greenhouses, Geothermics 111 (2023) 102718, https://doi.org/10.1016/j.geothermics.2023.102718.
[22] I.R. Andrade, E.D. dos Santos, H. Zhang, L.A.O. Rocha, A.L. Razera, L.A. Isoldi, Multi-objective numerical analysis of horizontal rectilinear earth–air heat exchangers with elliptical cross section using constructal design and TOPSIS, Fluids 9 (11) (2024) 257, https://doi.org/10.3390/fluids9110257.
[23] E.M. El-Said, M.A. Sharaf, A. Aljabr, S.A. Marzouk, Enhancing the performance of an earth air heat exchanger with novel pipe configurations, Int. J. Heat Fluid Flow 110 (2024) 109630, https://doi.org/10.1016/j.ijheatfluidflow.2024.109630.
[24] A. Alikhani, M. Maerefat, S.M.J. Sobhani, Analytical investigation on the optimal tube length of earth-to-air heat exchanger (EAHE), Geothermics 127 (2025) 103250, https://doi.org/10.1016/j.geothermics.2025.103250.
[25] S. Jiang, S. Dong, L. Ni, Performance of earth to air heat exchanger under freezing soil conditions, Appl. Therm. Eng. 262 (2025) 125269, https://doi.org/10.1016/j.applthermaleng.2024.125269.
[26] C.L. Hwang, K. Yoon, Methods for multiple attribute decision making, in: Multiple attribute decision making: methods and applications a state-of-the-art survey, 1981, pp. 58–191, https://doi.org/10.1007/978-3-642-48318-9_3.
[27] E.H.T. Cunegatto, F.S.F. Zinani, S.J. Rigo, Multi-objective optimization of micromixer design using genetic algorithms and multi-criteria decision-making algorithms, Int. J. Hydromechatron. 7 (3) (2024) 224–249, https://doi.org/10.1504/IJHM.2024.140573.
[28] A.L. Razera, R.J.C.D. Fonseca, L.A. Isoldi, E.D. dos Santos, L.A.O. Rocha, C. Biserni, Evolutionary design investigation applied to mixed convection heat transfer flows over semi-elliptical blocks inserted into a rectangular channel, Int. J. Hydromechatron. 7 (3) (2024) 196–223, https://doi.org/10.1504/IJHM.2024.140567.
[29] H.C. Cui, C.Y. Shi, M.J. Yu, Z.K. Zhang, Z.C. Liu, W. Liu, Optimal parameter design of a slot jet impingement/microchannel heat sink base on multi-objective optimization algorithm, Appl. Therm. Eng. 227 (2023) 120452, https://doi.org/10.1016/j.applthermaleng.2023.120452.
[30] N. Sun, S. Zhang, P. Jin, N. Li, S. Yang, Z. Li, F. Zhao, An intelligent plate fin-and-tube heat exchanger design system through integration of CFD, NSGA-II, ANN and TOPSIS, Expert Syst. Appl. 233 (2023) 120926, https://doi.org/10.1016/j.eswa.2023.120926.
[31] A. Bejan, Convection Heat Transfer, John Wiley & sons, 2013.
[32] B. Launder, D.B. Spalding, Lectures in Mathematical Models of Turbulence, Academic Press, London, 1972.
[33] D.C. Wilcox, Turbulence Modeling for CFD, DCW Industries, USA, 2002.
[34] D.W. Hahn, M.N. Özisik, Heat Conduction, John Wiley e Sons, 2012.
[35] M.K. Rodrigues, R. da Silva Brum, J. Vaz, L.A.O. Rocha, E.D. dos Santos, L.A. Isoldi, Numerical investigation about the improvement of the thermal potential of an earth-air heat exchanger (EAHE) employing the constructal design method, Renew. Energy 80 (2015) 538–551, https://doi.org/10.1016/j.renene.2015.02.041.
[36] S.R. Brum, J. Vaz, L.A.O. Rocha, E.D. dos Santos, L.A. Isoldi, A new computational modeling to predict the behavior of earth-air heat exchangers, Energ. Buildings 64 (2013) 395–402, https://doi.org/10.1016/j.enbuild.2013.05.032.
[37] V. Bansal, R. Misra, G.D. Agrawal, J. Mathur, Performance analysis of earth–pipe–air heat exchanger for winter heating, Energ. Buildings 41 (11) (2009) 1151–1154, https://doi.org/10.1016/j.enbuild.2009.05.010.
[38] V. Bansal, R. Misra, G.D. Agrawal, J. Mathur, Performance analysis of earth–pipe–air heat exchanger for summer cooling, Energ. Buildings 42 (5) (2010) 645–648, https://doi.org/10.1016/j.enbuild.2009.11.001.
[39] H.K. Versteeg, W. Malalasekera, An Introduction to Computational Fluid Dynamics: The Finite *Volume Method*, Pearson Education, 2007.
[40] S. Patankar, Numerical Heat Transfer and Fluid Flow, Taylor & Francis, 2018.
[41] C.R. Maliska, Fundamentals of Computational Fluid Dynamics, Springer Nature Switzerland AG, Cham, Switzerland, 2023.
[42] D.S. Wilks, Statistical Methods in the Atmospheric Sciences, Academic press, 2011.
[43] P.J. Pritchard, J.W. Mitchell, Fox and Mcdonald's Introduction to Fluid Mechanics, John Wiley & Sons, 2016.
[44] H. Schlichting, K. Gersten, Boundary-Layer Theory, Springer, 2016.
[45] S. Ali, Pressure drop correlations for flow through regular helical coil tubes, Fluid Dyn. Res. 28 (4) (2001) 295, https://doi.org/10.1016/S0169-5983(00)00034-4.
[46] ABNT, ABNT NBR 16401-2:2008, in: Central and unitary air conditioning systems, Part 2: Thermal Comfort, ABNT, Rio de Janeiro, Brazil, 2008.
[47] ASHRAE. *ASHRAE Handbook. Fundamentals - Chapter 8: Thermal Comfort*, ASHRAE, Atlanta-GA, USA.